

# DEVELOPMENT AND VALIDATION OF A NEW DRIFT FLUX MODEL IN ROD BUNDLE GEOMETRIES

**Ikuo Kinoshita and Toshihide Torige**

Institute of Nuclear Safety System, Inc.  
64 Sata, Mihama-cho, Mikata-gun, Fukui 919-1205, Japan  
kinoshita@inss.co.jp; torige.toshihide@inss.co.jp

**Minoru Yamada**

MHI Nuclear Engineering Co., Ltd.  
3-3-1 Minatomirai, Nishi-ku, Yokohama-city, Kanagawa 220-8401, Japan  
minoru2\_yamada@mnec.mhi.co.jp

**Takashi Hibiki**

School of Nuclear Engineering, Purdue University  
400 Central Drive, West Lafayette, IN 47907-2017, USA  
hibiki@purdue.edu

## ABSTRACT

In the authors' previous studies, low flow data were taken systematically from the Purdue University rod bundle facility at atmospheric pressure with air and water as working fluids. The data set was used to develop a new drift flux correlation for accident analyses to predict void fractions over a wide range of two-phase flow conditions in rod bundle geometries. In this study, the new correlation was implemented in the RELAP5/MOD3 code, and the void fraction prediction performance was compared with the EPRI correlation which was installed in the original RELAP5/MOD3 code. Numerical analyses carried out for the Purdue University rod bundle tests showed that the results obtained using the new correlation were in good agreement with the test data and represented an improvement over those obtained from the EPRI correlation. Numerical analyses carried out for the void profile tests in the THTF at ORNL, however, showed that the new correlation developed under low flow atmospheric pressure air/water conditions was less accurate for low flow high pressure steam/water conditions. The new correlation needs improvements in order to scale the pressure effects appropriately.

## KEYWORDS

Drift flux, Rod bundle, Void fraction, Low liquid flow, RELAP5

## 1. INTRODUCTION

Existing drift flux correlations for rod bundles may not appropriately consider two-phase flow mechanisms in low flow and low pressure conditions during accidents. For instance, at low liquid flow and low pressure conditions, downward flow at the outer perimeter has been observed in a large diameter pipe [1] and large concentrations of gas have been measured at the central higher velocity regions of large diameter channels [2]. These characteristics are attributed to recirculating flow patterns. Furthermore, large concentrations of void have been observed in the central regions of a rod bundle at low pressure and low flow conditions [3]. Therefore, similar to large diameter pipes, recirculating flow patterns may occur in rod bundles at low flow

and low pressure conditions. Low pressure systems introduce greater buoyancy forces because of an increased density difference between the continuous and dispersed phases. On the other hand, at high pressure and high liquid flow conditions, the decreased buoyancy forces and increased turbulence would prohibit any recirculating flow patterns from developing in rod bundles. Earlier drift flux correlations for rod bundles may have placed priority on use in high pressure and high liquid flow conditions because these are more representative of a prototypic power plant. This may provide an explanation for why recirculating flow patterns have not been previously considered for drift flux models in rod bundles. However, it may be important for a rod bundle drift flux correlation to consider these two-phase flow mechanisms. For instance, low flow and low pressure conditions are relevant for a loss-of-coolant accident (LOCA) or a loss-of-RHRS (residual heat removal systems) event during mid-loop operation.

In the authors' previous studies [4, 5], low flow data were taken systematically from the well-scaled Purdue University 8 x 8 rod bundle facility at atmospheric pressure with air and water as working fluids. Results indicated a significant increase in the distribution parameter when mixture volumetric flux was relatively low. The collected data were used to develop a new drift flux correlation for accident analyses to predict void fractions over a wide range of two-phase flow conditions in rod bundle geometries. The Hibiki and Ishii correlation for drift velocity [6] that reflected the effects of recirculating flow patterns was implemented in the new correlation. The distribution parameter was then back calculated from the one-dimensional drift flux model general expression using the drift velocity and the associated data. It was confirmed that the distribution parameter increased at low volumetric flux conditions before exponentially decreasing as superficial velocity increased, and approached asymptotically to a constant value which matched the distribution parameter determined for rod bundles at high flow and high pressure conditions. These characteristics were associated with recirculation flow patterns. A performance analysis demonstrated that the new correlation improved upon existing correlations and had an average relative error of  $\pm 4.5\%$  when predicting the void fraction of the database utilized in this work.

In this study, the new correlation is implemented in the RELAP5/MOD3 code [7], and numerical analyses are carried out for the Purdue University rod bundle experiments to investigate the applicability of the new correlation to the RELAP5 code. In addition, numerical analyses are carried out for the two-phase mixture level swell tests in the Thermal Hydraulic Test Facility (THTF) at the Oak Ridge National Laboratory (ORNL) [8, 9] to investigate the applicability of the new correlation to low liquid flow and high pressure conditions expected in a small break LOCA.

## 2. THE NEW DRIFT FLUX MODEL IN ROD BUNDLES

### 2.1. Overview of the New Rod Bundle Correlation Development

The drift flux model [10] is given by

$$\frac{\langle j_g \rangle}{\langle \alpha \rangle} = \langle \langle v_g \rangle \rangle = C_0 \langle j \rangle + \langle \langle V_{gj} \rangle \rangle, \quad (1)$$

where  $v_g$ ,  $\alpha$ ,  $j_g$ ,  $C_0$ ,  $j$ , and  $V_{gj}$  are gas velocity, void fraction, gas volumetric flux, distribution parameter, mixture volumetric flux, and drift velocity, respectively. The  $\langle \rangle$  and  $\langle \langle \rangle \rangle$  notations designate area-averaged and area-averaged void weighted mean values, respectively. In general, closure relations for the distribution parameter and the drift velocity are developed for application in certain flow regimes, geometries, fluid parameters or conditions, etc. Much work has been dedicated towards calculating drift flux parameters at various conditions. In order to develop the

new correlation that accounts for two-phase flow mechanisms at low flow and low pressure conditions, the data reported from Clark et al. [4] were utilized which were collected systematically from the well-scaled 8 x 8 rod bundle facility at atmospheric pressure low flow conditions with air and water as working fluids. The drift velocity was determined for the data by using the correlation by Hibiki and Ishii [6]. Hibiki and Ishii formulated the drift velocity correlation for large flow channels that spans stagnant to high liquid flow conditions. A significant attribute of their correlation is that gas velocity, namely void fraction, is used to appropriately scale the effect of recirculating flow patterns at low flow conditions on drift velocity. The distribution parameter was then back calculated from Eq. (1) using the drift velocity and the associated data.

Figure 1 shows the distribution parameter values obtained from the low flow and low pressure data [5]. Here the superscript + designates a non-dimensional value by considering bubble rise velocity which is given by the denominator in Eq. (2).

$$\langle j^+ \rangle = \langle j \rangle / (\sigma g \Delta \rho / \rho_f^2)^{1/4}, \quad \langle j_f^+ \rangle = \langle j_f \rangle / (\sigma g \Delta \rho / \rho_f^2)^{1/4} \quad (2)$$

As shown in Fig. 1, the distribution parameter first increases at low volumetric flux conditions before exponentially decreasing as volumetric flux increased, and approaches asymptotically to a constant value. These regions may be characterized by differing two-phase flow structures. The initial increase in the distribution parameter towards a maximum value,  $C_{\infty \max}$ , may be attributed to an increasing concentration of gas in the high velocity (central) regions of the flow channel and downward liquid flow at the outer perimeter. On the other hand, increasing the flow rate beyond the conditions for  $C_{\infty \max}$  enhances co-current flow which would effectively decrease the distribution parameter. This decrease approaches a constant value designated as  $C_{j\infty}$ . From the data trend, the value of  $C_{j\infty}$  is approximately 1.1, which matches the distribution parameter determined by Ozaki et al. [11] for rod bundles at prototypic conditions. The mixture volumetric flux condition at which  $C_{\infty \max}$  occurs is referred to here as  $\langle j^+ \rangle_{C_{\infty \max}}$ . As liquid volumetric flux increases,  $\langle j^+ \rangle_{C_{\infty \max}}$  increases, and  $C_{\infty \max}$  decreases. These transitions are expected to be related to changes in two-phase flow structure.

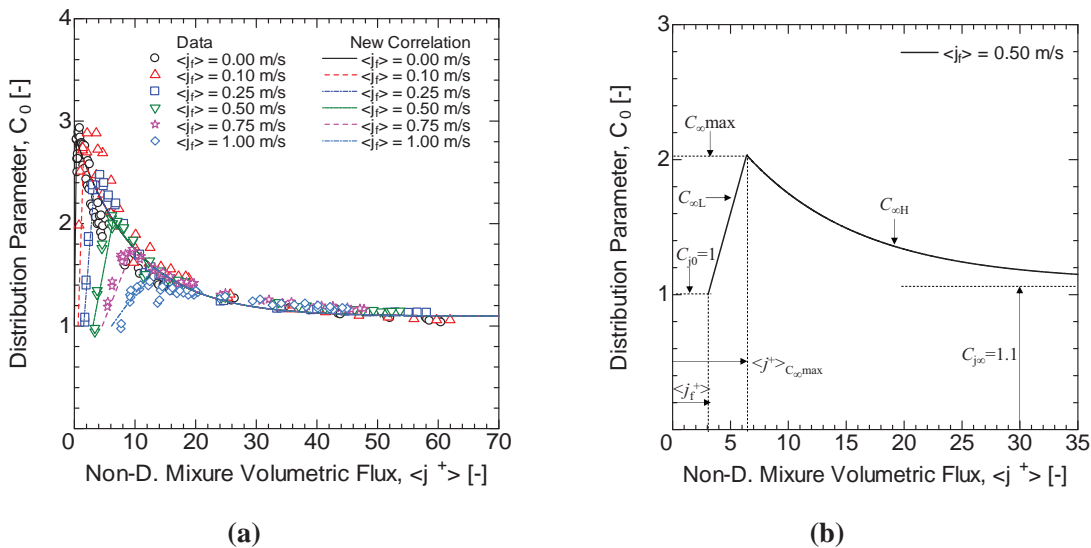


Figure 1. Distribution parameter (a) data and (b) schematic illustration [5].

**Table I. The new drift-flux correlation for rod bundles [5]**

$\langle\langle V_{gj}^+ \rangle\rangle = \langle\langle V_{gj,B}^+ \rangle\rangle e^{(-1.39\langle j_g^+ \rangle)} + \langle\langle V_{gj,P}^+ \rangle\rangle \left(1 - e^{(-1.39\langle j_g^+ \rangle)}\right)$ Hibiki and Ishii [6]	
$C_0 = C_\infty - (C_\infty - 1) \sqrt{\frac{\rho_g}{\rho_f}}$ Ishii [12]	$C_\infty = \begin{cases} C_{\infty L} & \text{for } \langle j^+ \rangle \leq \langle j^+ \rangle_{C_\infty \max} \\ C_{\infty H} & \text{for } \langle j^+ \rangle > \langle j^+ \rangle_{C_\infty \max} \end{cases}$
$C_{\infty H}(\langle j^+ \rangle) = 1.1 + 1.84e^{-0.100\langle j^+ \rangle}$	$C_{\infty L} = \left[ \frac{C_{\infty H}(\langle j^+ \rangle_{C_\infty \max}) - C_{j0}}{\langle j^+ \rangle_{C_\infty \max} - \langle j_f^+ \rangle} \right] \langle j_g^+ \rangle + C_{j0}$
$\langle j^+ \rangle_{C_\infty \max} = m \langle j_f^+ \rangle + b$	$m = \frac{1}{1 - \langle \alpha \rangle_{crit} C_0}; \quad b = \frac{\langle\langle V_{gj}^+ \rangle\rangle \langle \alpha \rangle_{crit}}{1 - \langle \alpha \rangle_{crit} C_0}$
$\langle \alpha \rangle_{crit} = \min(0.0284 \langle j_f^+ \rangle + 0.125, 0.52)$	

For the new correlation, the distribution parameter was approximated by a linear increasing and exponential decreasing region as show schematically in Fig. 1 (b). A boundary condition was used to distinguish between each region as

$$C_\infty = \begin{cases} C_{\infty L} & \text{for } \langle j^+ \rangle \leq \langle j^+ \rangle_{C_\infty \max} \\ C_{\infty H} & \text{for } \langle j^+ \rangle > \langle j^+ \rangle_{C_\infty \max} \end{cases} \quad (3)$$

As gas volumetric flux degreased to zero, the initial distribution parameter was set to  $C_{j0} = 1.0$ . This represented an even distribution of void fraction over the rod bundle cross section. On the other hand, the exponential decrease was described using a least squares curve fitting approach.

$$C_{\infty H}(\langle j^+ \rangle) = 1.1 + 1.84e^{-0.100\langle j^+ \rangle} \quad (4)$$

The transition condition in Fig. 1 was associated with a critical void fraction,  $\langle \alpha \rangle_{crit}$ , corresponding to a transition in the two-phase structure. The relationship between critical void fraction and dimensionless liquid volumetric flux was approximated by

$$\langle \alpha \rangle_{crit} = \min(0.0284 \langle j_f^+ \rangle + 0.125, 0.52) \quad (5)$$

The relationship between  $\langle j^+ \rangle_{C_\infty \max}$  and  $\langle j_f^+ \rangle$  was determined by the critical void fraction and the drift-flux general expression (1) as follows.

$$\langle j^+ \rangle_{C_\infty \max} = m \langle j_f^+ \rangle + b \quad (6)$$

$$m = \frac{1}{1 - \langle \alpha \rangle_{crit} C_0}; \quad b = \frac{\langle \langle V_{gj}^+ \rangle \rangle \langle \alpha \rangle_{crit}}{1 - \langle \alpha \rangle_{crit} C_0} \quad (7)$$

Finally, it was necessary to scale the distribution parameter based on fluid properties or system pressure. This was done by incorporating the correlation by Ishii [12]. The new correlation is detailed in Table I.

## 2.2. Performance Analysis

The drift-flux correlations are compared against the low liquid velocity and low pressure data [4]. A comparison between the void fractions predicted by the new correlation and the measured values is shown in Fig. 2(a). Here, there are no distinct biases present in void fraction prediction by the new correlation and the random error is mostly within the  $\pm 10\%$  error band.

A comparison between the void fractions predicted by the EPRI correlation [13] and the measured values is shown in Fig. 2(b). The EPRI correlation, also known as the Chexal-Lellouche correlation, was developed to cover the full range of conditions in rod bundles and implemented in the RELAP5/MOD3 code. Disagreement is observed between the EPRI correlation and data trends at lower void fractions. This error may be attributed to the empirical relations of the EPRI correlation not appropriately considering secondary flow patterns.

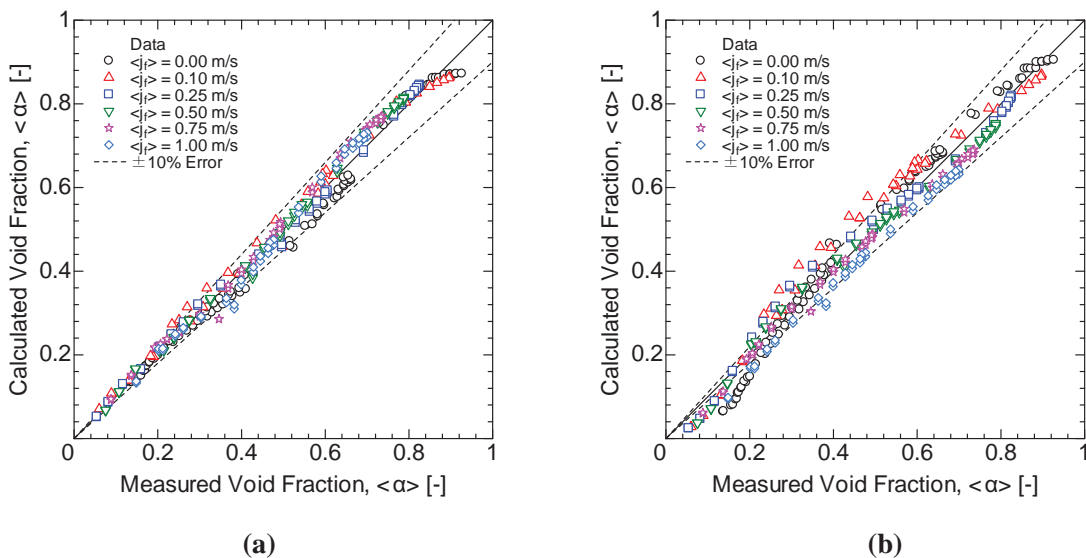


Figure 2. Void fraction prediction error [5]; (a) the new correlation and (b) the EPRI correlation.

## 3. PURDUE UNIVERSITY ROD BUNDLE TEST ANALYSES

The new correlation is implemented in the RELAP5/MOD3 code, and numerical analyses were carried out for the Purdue University rod bundle tests [4] to investigate the applicability of the new correlation to the RELAP5 code. The analysis results are compared with those by the EPRI correlation implemented in the original RELAP5 code.

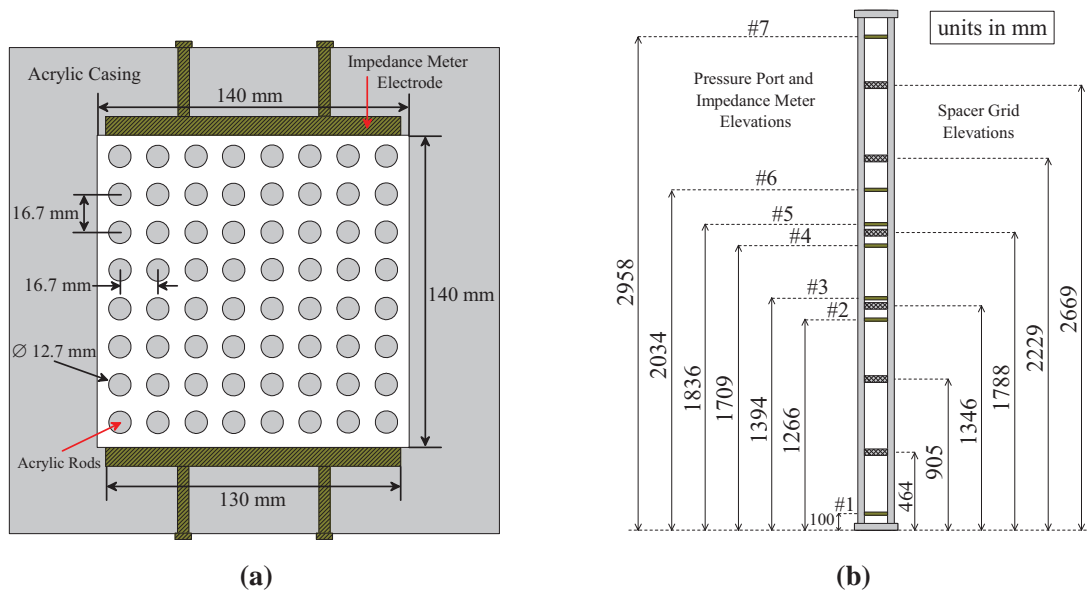


Figure 3. Rod bundle test section [4]; (a) cross sectional view and (b) axial view.

### 3.1. Outline of Purdue University Rod Bundle Tests

Two-phase low flow data were taken systematically from a well-scaled 8 x 8 acrylic rod bundle test facility at atmospheric pressure with air and water as working fluids [4]. Figure 3 shows the rod bundle test section as (a) cross-sectional view and (b) axial view. The casing of the rod bundle was made of transparent acrylic plates in a 140 x 140 mm square duct. The acrylic rods had a diameter of 12.7 mm and a pitch of 16.7 mm. There were 7 spacer grids located along the length of the test section to limit vibration and simulate spacers in the prototypic design. The impedance meters 1 – 7 were located at  $z/D_{H, Case} = 0.7, 9.0, 10.0, 12.2, 13.1, 14.5,$  and  $21.1$ , respectively. The seven pressure ports were at the same locations. The height of the test facility was 3 m. Area average void fraction measurements were performed using impedance meters 4 and 6. These locations were far enough downstream from the spacer grids so that their effect of interfacial structure was negligible [4]. The six different liquid flow conditions utilized were  $j_f = 0.00, 0.10, 0.25, 0.50, 0.75, 1.00$  m/s.

### 3.2. Analysis Methods

Nodalization for the analyses is shown in Fig. 4. The bundle domain was represented by a RELAP5 pipe component divided into 26 volumes. The part of the test section was represented by fine node from impedance meters 4 to 6. To inject water and air into the bottom of the bundle domain, time-dependent volumes and time-dependent junctions were connected to the bottom of the bundle domain. The injection flow rates were controlled so that the liquid and gas volumetric fluxes at the measuring position matched those

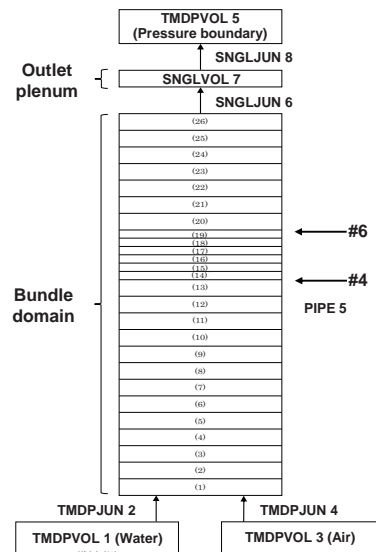


Figure 4. Nodalization for the analyses.

of the tests. The injected water and air temperature were the same as the tests. The outlet plenum was simulated by a single volume. To get a free outflow boundary condition, the time-dependent volume and a normal junction were connected to the outlet plenum. The pressure was the same as that of the test. Analysis cases in this study are listed in Table II.

**Table II. Analysis Cases**

Series No.	Measured $j_f$ [m/s]	Measured $j_g$ [m/s]	Measured void fraction [-]
Series 1	0.00	0.06 – 2.12	0.14 – 0.60
Series 2	1.01 – 1.02	0.25 – 6.33	0.15 – 0.70

### 3.3. Analysis Results

#### 3.3.1. Series 1 ( $j_f = 0.00$ m/s, $j_g = 0.0629$ m/s)

Figure 5(a) compares the predicted void fraction profiles by the new and the EPRI correlations for the test carried out at  $j_f = 0.00$  m/s,  $j_g = 0.0629$  m/s. When the axial positions become higher, the predicted void fractions slightly increase. This is because the gas pressures are lower at the higher axial position. In this sense, the RELAP5 code implementing the new correlation makes a reasonable prediction as well as the EPRI correlation. In Fig. 5(a), the measured void fraction at the position of the impedance meters #4 is also plotted. The void fraction predicted by the new correlation is within the  $\pm 10\%$  error band of the measured value. On the other hand, the void fraction predicted by the EPRI correlation is below the  $\pm 10\%$  error band of the measured value.

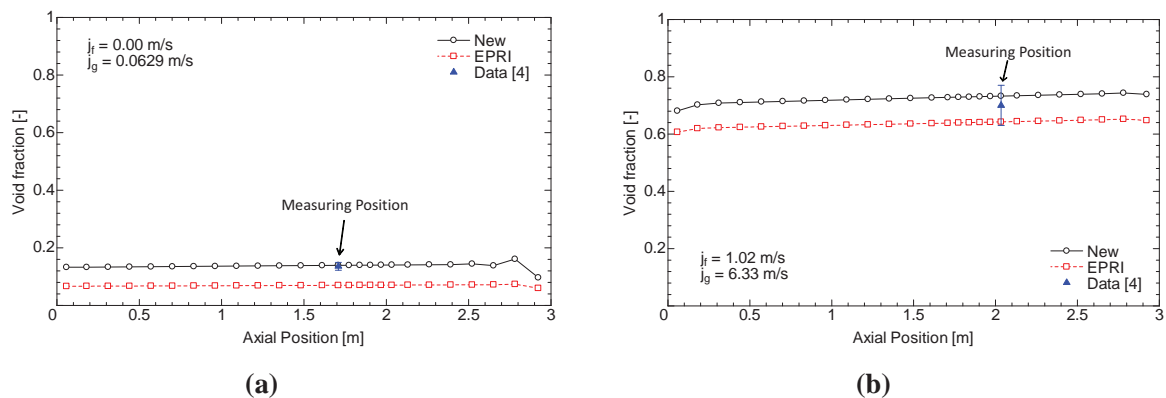
#### 3.3.2. Series 2 ( $j_f = 1.02$ m/s, $j_g = 6.33$ m/s)

Figure 5(b) compares the predicted void fraction profiles by the new and the EPRI correlations for the test carried out at  $j_f = 1.02$  m/s,  $j_g = 6.33$  m/s. As is Fig. 5(a), when the axial positions become higher, the predicted void fractions slightly increase. This case also shows that the RELAP5 code implementing the new correlation makes a reasonable prediction as well as the EPRI correlation. In Fig. 5(b), the measured void fraction at the position of the impedance meters #6 is also plotted. Although both the void fractions predicted by the new correlation and the EPRI correlation are within the  $\pm 10\%$  error band of the measured value, the new correlation makes a better prediction than the EPRI correlation.

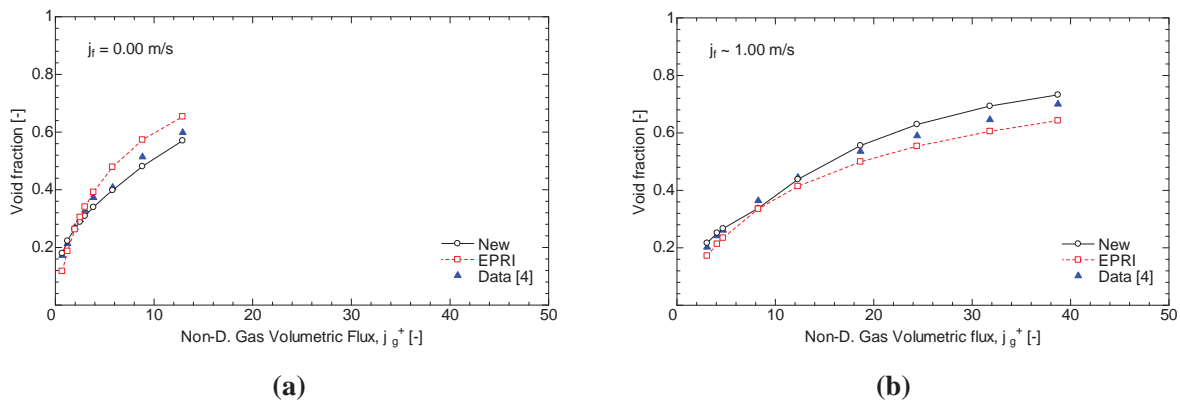
#### 3.3.3. Void fraction prediction

Figure 6 compares the predicted void fractions by the new and the EPRI correlations, arranged along with the non-dimensional gas volumetric fluxes. In the case of Series 1 ( $j_f = 0.00$  m/s), the new correlation leads to better agreement with the data than the EPRI correlation. This is because the new correlation appropriately considers two-phase flow mechanisms in stagnant liquid flow conditions.

On the other hand, in the case of Series 2 ( $j_f \sim 1.00$  m/s), there is no significant difference in the void fraction prediction accuracy between the new and the EPRI correlations. This may be due to the recirculating flow pattern being diminished at high flow conditions. In fact, as shown in Fig. 1(a), the increase of the distribution parameter at  $j_f = 1.00$  m/s is not so significant compared to that at  $j_f = 0.00$  m/s.



**Figure 5. Predicted void fraction profiles (a) Series 1 ( $j_f = 0.00$  m/s,  $j_g = 0.0629$  m/s) and (b) Series 2 ( $j_f = 1.02$  m/s,  $j_g = 6.33$  m/s). Measured void fractions are also plotted with the  $\pm 10\%$  error band.**



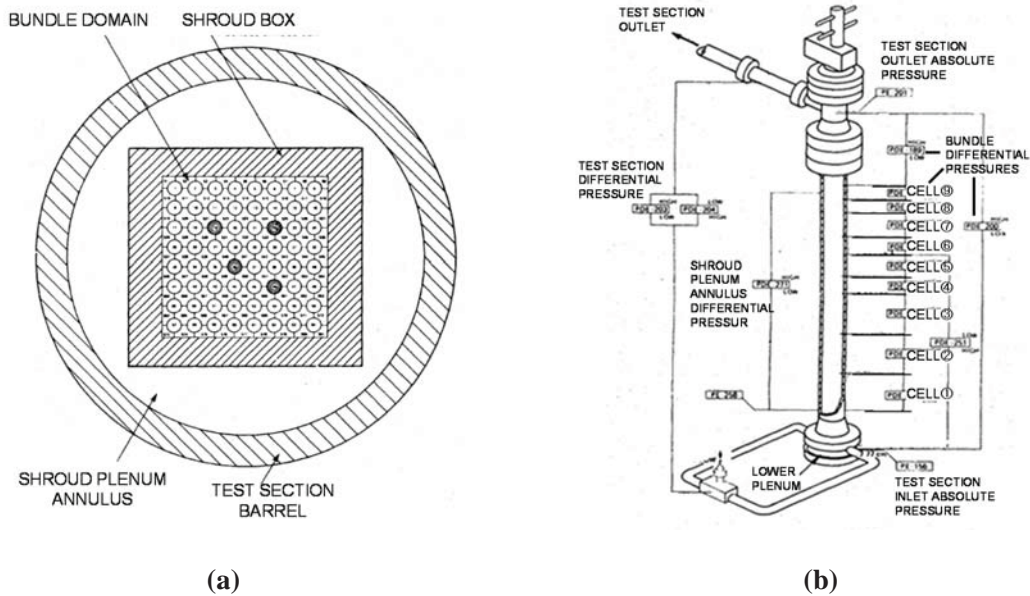
**Figure 6. Void fraction prediction (a) Series 1 and (b) Series 2.**

#### 4. ORNL/THTF ROD BUNDLE TEST ANALYSES

To investigate the applicability of the new correlation to low liquid flow and high pressure conditions expected in a small break LOCA, the numerical analyses by the RELAP5 code implementing the new correlation were conducted for the ORNL/THTF void profile tests [8, 9]. The analysis results are compared with those by the original RELAP5 code with the EPRI correlation.

##### 4.1. Outline of ORNL/THTF Void Profile Tests

The THTF is a high pressure bundle thermal-hydraulics loop, and designed to produce a thermal-hydraulic environment similar to that expected in a small break LOCA. Figure 7(a) shows a sectional view of the THTF test section. The test section consisted of the bundle domain, shroud box, shroud-plenum annulus, and test section barrel. The bundle domain consisted of 60 heated rods and 4 unheated rods, their pitches were 1.27cm. The outside diameter of all heated rods was 0.95cm. These are the same values as typically used for a 17 x 17 fuel assembly. The heated rods had a heater surrounded by boron nitride, and a stainless steel sheath outside. The axial void fraction profiles were obtained from differential pressure measurements.



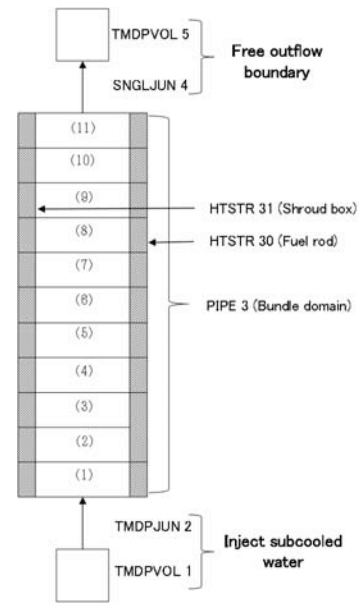
**Figure 7. Rod bundle test section of the THTF [8]; (a) cross-sectional view and (b) pressure instrumentation.**

Figure 7(b) indicates locations of those measurements. The bundle domain was divided into 9 differential pressure cells along the axis length. The volume average void fractions were obtained at the mid-heights of the differential pressure cell measurements. As for differential pressure cells including the beginning of the boiling length, the void fractions were obtained at the mid-heights of the two-phase regions of the cells.

The void profile tests were started by boiling off water from the bundle, which was originally filled with water. On reaching the quasi-steady state, subcooled water was supplied from the bundle domain bottom in order to compensate for the amount of transpiration from the bundle domain top, and the bundle was uncovered partially.

#### 4.2. Analysis Methods

Nodalization for the analyses is shown in Fig. 8. The bundle domain (simulated heated region only) was divided into volumes corresponding to the differential pressure cells, so that the volume center positions became the void fraction evaluation positions. The differential pressure cells which included the beginning of the boiling length were also divided by the beginning of the boiling length. The heated rods and the shroud box surrounding the bundle domain were simulated as the heat structure. The fractional heat loss from the shroud box was evaluated in the tests. In the analyses the heat loss was simulated assuming that it was axially uniform.



**Figure 8. Nodalization for the analyses.**

To inject subcooled water into the bottom of the bundle domain, a time-dependent volume and a time-dependent junction were connected to the bottom of the bundle domain. The injection flow rate was controlled so that the collapsed water level of the bundle domain matched that of the test, and the injected water temperature was the same as the test. To get a free outflow boundary condition, the time-dependent volume and a normal junction were connected to the top of the bundle domain. The pressure of the top of the bundle domain was the same as that of the test. Analysis cases in this study are listed in Table III.

**Table III. Analysis Cases**

Test No.	Fluids (gas/liquid)	Pressure [MPa]	Power [kW/m]
<b>Test 3.09.10J</b>	steam/water	4.20	1.07
<b>Test 3.09.10K</b>	steam/water	4.01	0.32
<b>Test 3.09.10M</b>	steam/water	6.96	1.02
<b>Test 3.09.10N</b>	steam/water	7.08	0.47
<b>Test 3.09.10AA</b>	steam/water	4.04	1.27
<b>Test 3.09.10BB</b>	steam/water	3.86	0.64
<b>Test 3.09.10CC</b>	steam/water	3.59	0.33
<b>Test 3.09.10DD</b>	steam/water	8.09	1.29
<b>Test 3.09.10EE</b>	steam/water	7.71	0.64
<b>Test 3.09.10FF</b>	steam/water	7.53	0.32

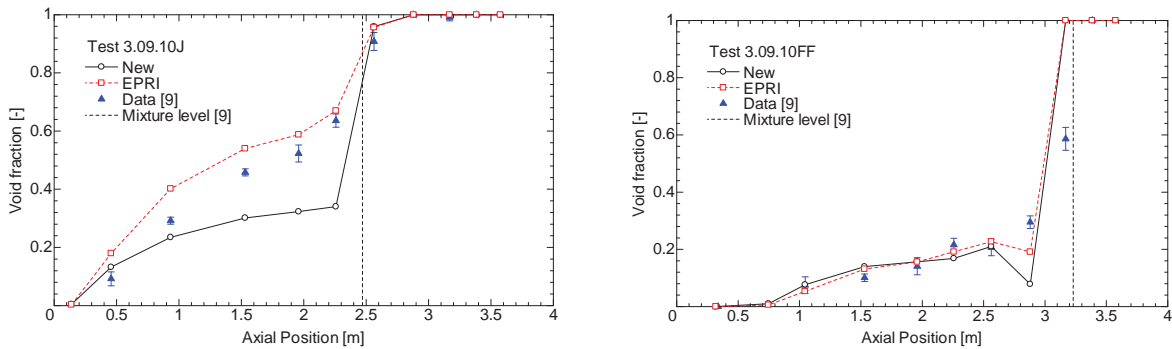
### 4.3. Analysis Results

#### 4.3.1. Test 3.09.10J

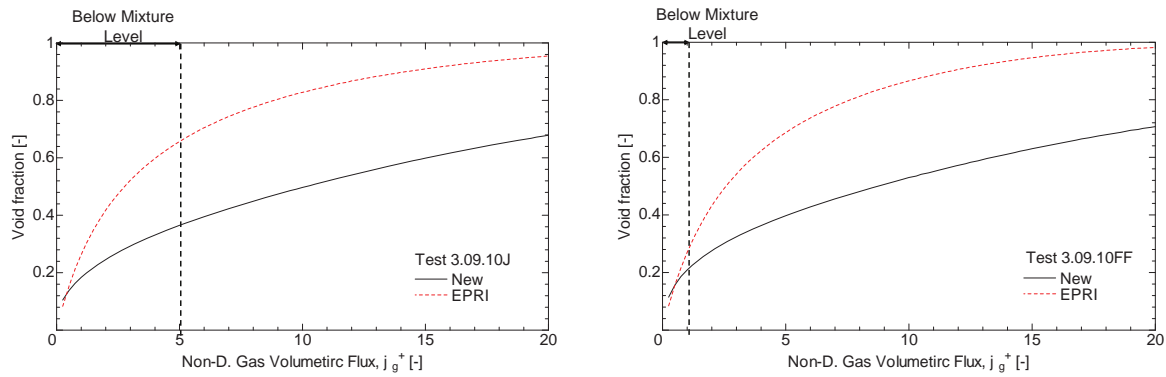
The analysis results of void fraction profiles for Test 3.09.10J are shown in Fig. 9(a). The difference of void fraction predictions between the new correlation and the EPRI correlation becomes larger when the axial positions become higher. This difference can be understood by the relation between void fractions and steam volumetric fluxes. Figure 10(a) presents the void fractions obtained by applying the new correlation and the EPRI correlation directly, arranged according to non-dimensional gas volumetric fluxes. Under the test conditions, non-dimensional steam volumetric fluxes are in the range 0 – 5. For this range, the difference of void fraction predictions becomes larger when the gas volumetric fluxes become larger. The void fractions calculated by the new correlation tend to be under-predicted compared with the measured data. Similar results are obtained for simulations of test 3.09.10M, AA, BB, CC, DD and EE.

#### 4.3.2. Test 3.09.10FF

The analysis results of void fraction profiles for Test 3.09.10FF are shown in Fig. 9(b). In this case, there is no significant difference of the void fraction prediction between the new correlation and the EPRI correlation, and both correlations give good agreement with the data. Figure 10(b) presents the void fractions obtained by applying the new correlation and the EPRI correlation directly, arranged according to non-dimensional gas volumetric fluxes. Using the test conditions, non-dimensional gas volumetric fluxes are in the range 0 – 1. For this range, there is no significant difference between the correlations, and both the correlations lead to similar results and give good agreement with the data. Similar results are obtained for simulations of tests 3.09.10K and N.



(a) (b)  
**Figure 9. Predicted void fraction profiles (a) Test 3.09.10J and (b) Test 3.09.10FF.**



(a) (b)  
**Figure 10. Void fractions obtained by applying the new correlation and the EPRI correlation directly (a) Test 3.09.10J and (b) Test 3.09.10FF.**

### 4.3.3. Void fraction prediction

Figure 11(a) compares the predicted void fractions by the new correlation and the EPRI correlation versus the void fractions measured in the ORNL/THTF tests. The void fractions obtained using the new correlation are under-estimated for most of the cases. Figure 11(b) shows the drift flux plane. The gas velocities predicted by the new correlation tend to reach those by the EPRI correlation when system pressures increase. This tendency indicates that the new correlation developed under low flow atmospheric pressure air/water conditions is less accurate for low flow high pressure steam/water conditions.

## 5. DISCUSSION

Figure 12 shows the behavior of the new correlation as it is scaled to the typical BWR pressure,  $P = 7$  MPa, and PWR pressure,  $P = 15.5$  MPa, reproduced from figures in [5].

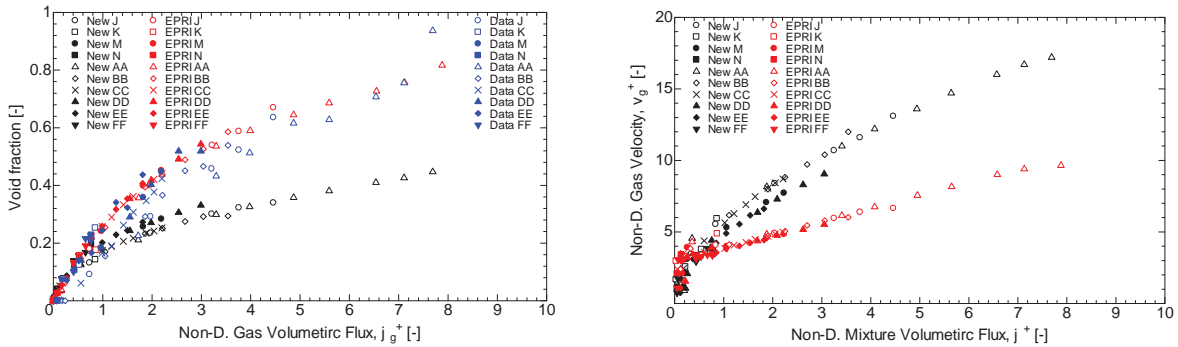


**Figure 11. All cases (a) void fraction prediction (b) gas velocity prediction. Open symbols represent the data obtained by the tests conducted under pressures of about 4.0 MPa, while filled symbols the data by the tests under pressures of about 7.5 MPa.**

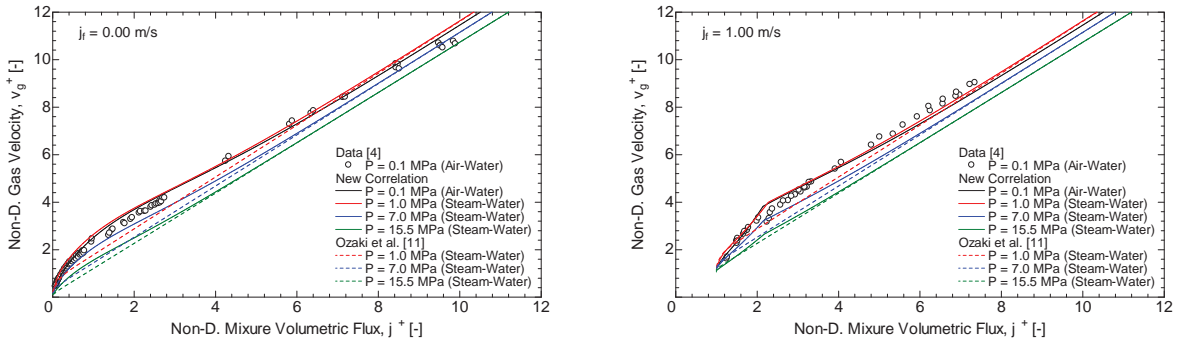


**Figure 12. Behavior of the new correlation at plant-scale conditions [5]; (a)  $j_f = 0.00$  m/s and (b)  $j_f = 1.00$  m/s. Values obtained with the correlation of Ozaki et al. [11] are also plotted.**

As pressure increases, the distribution parameter becomes relatively constant and approaches the value of the Ozaki et al. [11] correlation, which was developed with regard to primarily high pressure data. However, there remains a difference between them, which may be because the distribution parameter  $C_\infty$  of the new correlation does not properly scale the physical effects under high pressure conditions. The new correlation needs improvements in order to scale the pressure effects appropriately.

**6. CONCLUSIONS**

Existing drift flux correlations for rod bundles may have placed priority on use in high pressure and high liquid flow conditions because these are more representative of a prototypic power plant. Therefore, recirculating flow patterns which may occur at low pressure and low flow conditions have not been previously considered for drift flux model in rod bundles. However, it may be important for a rod bundle drift flux correlation to consider these two-phase flow mechanisms because, for instance, low flow and low pressure conditions are relevant for a LOCA or a loss-of-RHRS event during mid-loop operation.

In this study, a new correlation was implemented in the RELAP5/MOD3 code, and the void fraction prediction performance was compared with the EPRI correlation which was installed in the original RELAP5/MOD3 code. Numerical analyses carried out for the Purdue University rod bundle tests showed that the results obtained using the new correlation were in good agreement with the test data and represented an improvement over those obtained from the EPRI correlation. Numerical analyses carried out for the void profile tests in the THTF at ORNL showed that the new correlation developed under low flow atmospheric pressure air/water conditions was less accurate for low flow high pressure steam/water conditions. The distribution parameter of the new correlation needs improvements in order to scale the pressure effects appropriately.

## REFERENCES

1. Ohnuki, A., Akimoto, H. and Sudo, Y., "Flow pattern and its transition in gas-liquid two-phase flow along large vertical pipe," *Proc. 2nd Int. Conf. Multiphase Flow*, Vol. 3, pp.17-23 (1995).
2. Ohnuki, A. and Akimoto, H., "An experimental study on developing air-water two-phase flow along a large vertical pipe: effect of air injection method," *International Journal of Multiphase Flow*, **22**, pp.1143-1154 (1996).
3. Paranjape, S., Ishii, M., and Hibiki, T., "Modeling and measurement of interfacial area concentration in two-phase flow," *Nuclear Engineering and Design*, **240**, pp.2329-2337 (2010).
4. Clark, C., Griffiths, M., Chen, S.W., Hibiki, T., Ishii, M., Kinoshita, I., and Yoshida, Y., "Experimental study of void fraction in a 8 x 8 rod bundle at low pressure and low liquid flow conditions," *International Journal of Multiphase Flow*, **62**, pp.87-100 (2014).
5. Clark, C., Griffiths, M., Chen, S.W., Hibiki, T., Ishii, M., Ozaki, T., Kinoshita, I., and Yoshida, Y., "Drift-flux correlation for rod bundle geometries," *International Journal of Heat and Fluid Flow*, **48**, pp.1-14 (2014).
6. Hibiki, T. and Ishii, M., "One-dimensional drift-flux model for two-phase flow in a large diameter pipe," *International Journal of Heat and Mass Transfer*, **46**, pp.1773-1790, (2003).
7. RELAP5/MOD3.3, *Code Manual Volume IV: Models and Correlations*, NUREG/CR-5535/Rev1, Prepared for the Division of Systems Research, Office of Nuclear Regulatory Research. USNRC by Information Systems Laboratories, Inc., Rockville, Maryland (2001).
8. Felde, D. K. et al., "Facility Description THTF MOD3 ORNL PWR BDHT Separate-Effects Program", NUREG/CR-2640 (1982).
9. Anklam, T. M. et al., "Experimental Investigations of Uncovered-Bundle Heat Transfer and Two-Phase Mixture-Level Swell Under High-Pressure Low-Heat-Flux Conditions", NUREG/CR-2456 (1982).
10. Zuber, N. and Findlay, J. A., "Average Volumetric Concentration in Two-Phase Flow Systems," *Journal of Heat Transfer*, **87**, pp.453-468 (1965).
11. Ozaki, T., Suzuki, R., Mashiko, H. and Hibiki, T., "Development of drift-flux model based on 8 x 8 BWR rod bundle geometry experiments under prototypic temperature and pressure conditions," *Journal of Nuclear Science and Technology*, **50**, pp.563-580 (2013).
12. Ishii, M., "One-Dimensional Drift-flux Model and Constitutive Equations for Relative Motion between Phases in Various Two-phase Flow Regimes," ANL-77-47, USA (1977).
13. Chexal, B. and Lellouche, G., *A Full-Range Drift-Flux Correlation for Vertical Flows (Revision 1)*, Electric Power Research Institute. EPRI-NP-3989-SR (1986).